

# Additional transition line in jammed asymmetric bidisperse granular packings

Juan C. Petit,<sup>1</sup> Nishant Kumar,<sup>1</sup> Stefan Luding,<sup>2</sup> and Matthias Sperl<sup>1,3</sup>

<sup>1</sup>*Institut für Materialphysik im Weltraum, Deutsches Zentrum für Luft- und Raumfahrt (DLR), 51170 Köln, Germany*

<sup>2</sup>*Multi-Scale Mechanics (MSM), Faculty of Engineering Technology,*

*MESA+, University of Twente, Enschede, The Netherlands*

<sup>3</sup>*Institut für Theoretische Physik, Universität zu Köln, 50937 Köln, Germany*

(Dated: February 7, 2020)

We present numerical evidence for an additional discontinuous transition inside the jammed regime for an asymmetric bidisperse granular packing upon compression. This additional transition line separates jammed states with networks of predominantly large particles from jammed networks formed by both large and small particles, and the transition is indicated by a discontinuity in the number of particles contributing to the jammed network. The additional transition line emerges from the curves of jamming transitions and terminates in an end-point where the discontinuity vanishes. The additional line is starting at a size ratio around  $\delta = 0.22$  and grows longer for smaller  $\delta$ . For  $\delta \rightarrow 0$ , the additional transition line approaches a limit that can be derived analytically. The observed jamming scenarios are reminiscent of glass-glass transitions found in colloidal glasses.

Jamming governs the transition to rigidity of athermal amorphous systems. Granular matter is one example showing its jamming density,  $\phi_J$ , at a packing fraction marked by a discontinuous jump in the contact number [1–6]. For frictionless monodisperse packings, such a value is close to  $\phi_J \approx 0.64$  in 3D [5, 7]. For bidisperse packings, introduced to consider a higher degree of complexity in the system and to suppress crystallization,  $\phi_J$  can be tuned to higher values by varying the size ratio,  $\delta$ , and volume concentration of small particles,  $X_S$ , [8–12]. This is relevant for industrial processes since mechanical properties of bidisperse packings such as bulk modulus and wave speed can be controlled [13].

Although the dependence of the jamming density on  $\delta$  and  $X_S$  has been studied previously [8–12], a better understanding of jammed states in highly asymmetric bidisperse mixtures for extremely low  $X_S$  is intended. For example, previous works have assumed that the jammed structure of a bidisperse packing is formed by the equal contribution of both large and small particles since both species jam simultaneously at  $\phi_J$  [9–11]. This is true above certain values of  $\delta$  and  $X_S$ , since then the particle sizes are similar enough and concentration of small particles is high enough that both species follow the same behavior. However, for lower values of  $\delta$  and  $X_S$ , each component behaves differently when approaching jamming, which suggests a decoupling in the jamming in the binary system. Indeed, it has been recently evidenced in Ref. [8] that the jammed structure of an extremely asymmetric bidisperse system evolves from a small-sphere-rich to a small-sphere-poor structure. Such behavior is marked by an abrupt decay in the number of small particles contributing to the jammed structure at a specific  $X_S$ , while the rest of small particles remain without contacts.

This indicates that in principle, two different pathways to jamming need to be distinguished for small  $\delta$ : one driven by predominantly large particles, and one driven by both together. Our aim in this letter is to demon-

strate that indeed, the distinction can be made rigorous by an analysis of the partial contact numbers between particles of different species. It leads in particular to the identification of a new transition between *different jammed states* for  $X_S < X_S^*$ .

To investigate the emergence of this new transition, we used MercuryDPM to perform 3D Discrete Element Method (DEM) simulations, suitable to study granular systems [14–16]. Here, we consider bidisperse packings formed by  $N = 6000$  particles, where a number of large,  $N_L$ , and small,  $N_S$ , particles with radius  $r_L$  and  $r_S$  are considered, respectively. We characterize each packing by the size ratio,  $\delta = r_S/r_L$ , and the volume concentration of small particles,  $X_S = N_S\delta^3/(N_L + N_S\delta^3)$ . We use the linear normal contact force model given as  $\mathbf{f}_{ij}^n = f_{ij}^n \hat{\mathbf{n}} = (k_n \alpha_c + \gamma_n \dot{\alpha}_c) \hat{\mathbf{n}}$  [13, 14, 17], where  $k_n$  is the contact spring stiffness,  $\gamma_n$  is the contact damping coefficient,  $\alpha_c$  is the contact overlap and  $\dot{\alpha}_c$  is the relative velocity in the normal direction  $\hat{\mathbf{n}}$ . An artificial background dissipation force,  $\mathbf{f}_b = -\gamma_b \mathbf{v}_i$ , proportional to the velocity  $\mathbf{v}_i$  of particle  $i$  is added, resembling the damping due to a background medium. We fix  $r_L = 1.5$  mm and vary  $r_S \in [0.255, 1.5]$  mm, such that  $\delta \in [0.15, 1]$ . Both small/large particles have the same interacting properties, i.e.,  $\rho = 2000$  kg/m<sup>3</sup>,  $k_n = 10^5$  kg/s<sup>2</sup> and  $\gamma_n = \gamma_b = 1$  kg/s, which represent glass beads since they are most spherical and easily available material in experiments. The contact duration,  $t_c$ , and restitution coefficient,  $e$ , depend on the particle sizes. The fastest response time scale corresponding to the interaction between smallest particles according to the lowest value of  $\delta$  is  $t_c = 0.013$   $\mu$ s and  $e = 0.996$ . As usual in DEM, the time step was chosen to be 50 times smaller than the shortest time scale  $t_c$ . The contact and background dissipation value is used to reduce computational time during relaxation. We restrict ourselves to isotropic deformation and the linear contact model without any friction between particles [18]. Thus, we exclude all the non-linearities

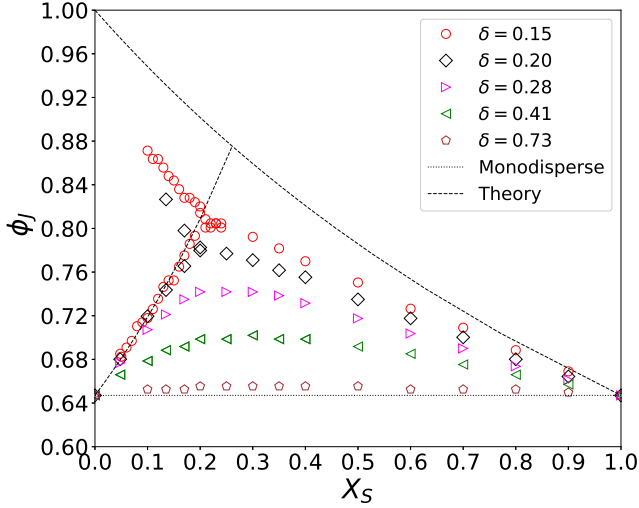


FIG. 1. Jamming density,  $\phi_J$ , as a function of the volume concentration of small particles,  $X_S$ , for different values of the size ratio,  $\delta$ . The extreme  $X_S$  values (0 and 1) correspond to monodisperse systems where  $\phi_J = \phi_{RCP} \approx 0.64$  indicated by the dashed horizontal line. Solid lines represents the analytical result of Eq. (1) [21].

present in the system due to contact models and analyze the effect of size and concentration at jamming.

Each bidisperse packing corresponding to a combination of  $(\delta, X_S)$  is created and further compressed using a unique, well defined protocol [19]. For each packing, configurations near (below and above) their jamming density are picked from the decompression branch. This is allowing packings to dissipate their kinetic energy and reach quickly unjammed, non-overlapping packings [20]. Therefore,  $\phi_J$  for each configuration is determined at the point where the partial mean contact number exhibits a sharp drop. Note that this protocol allows to identify multiple jamming densities occurring at different maximum packing fractions [12]. The values of  $\phi_J$  as a function of  $X_S$  for different  $\delta$  are shown in Fig. 1.

For a particular  $\delta$ , the jamming density increases with  $X_S$  up to a maximum value occurring at  $X_S^* \approx 0.21$ , then decreases for larger values. Along the increasing transition line, jamming is driven by the force network created by the large particles since most of the small ones remain without or only few contacts in the cages formed by the large ones. This is confirmed when looking at Fig. 2 (a,c), where mainly large particles are carrying the load in the jammed state. On the other hand, on the decreasing branch of  $\phi_J$  for high  $X_S$  small and large particles jam simultaneously at the same density, see Fig. 2 (b,d). However, for lower values of  $\delta$  and  $X_S$  a decoupling in the mean contact number,  $Z$ , between large and small particles is observed, see Fig. 2 (a). Large particles first jam at lower  $\phi$  while small ones remain without contacts. Making the packing denser, small particles exhibit an ap-

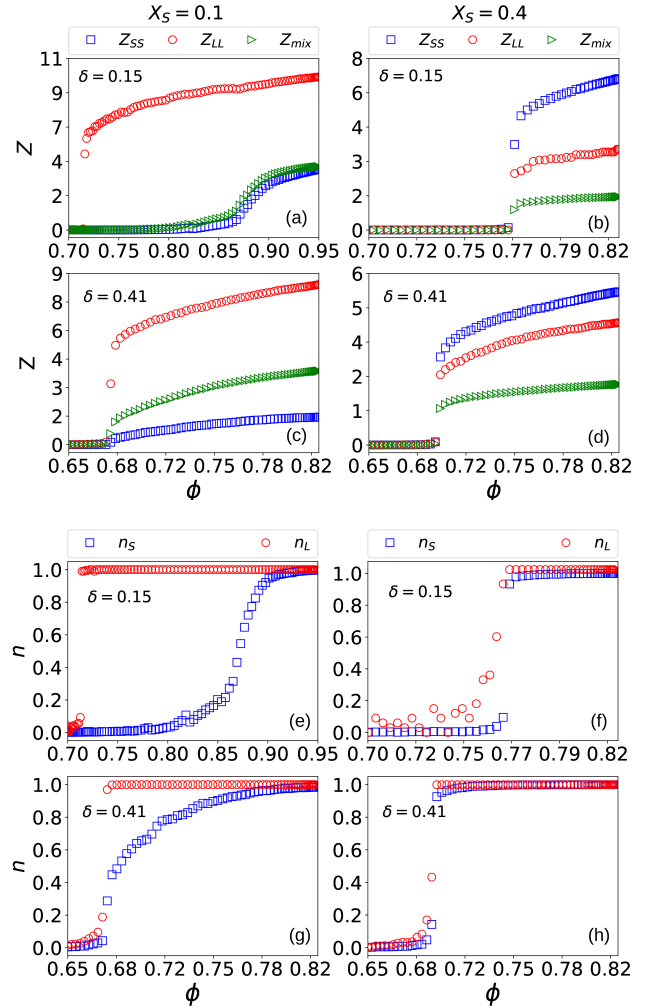


FIG. 2. (a-d) Mean contact number,  $Z$ , for each type of contact as a function of  $\phi$  for four tuples of  $\delta$  and  $X_S$ .  $Z_{nm}$  corresponds to the sum of contacts between particles  $n$  and  $m$  divided by total number of  $N_n$  particles, with  $n, m \in [L, S]$ . The analyzed data were along the decompression branch.  $Z_{mix}$  is defined as  $Z_{mix} = (Z_{LS} + Z_{SL})/N$ . (e-h) Fractions of large,  $n_L$ , and small,  $n_S$ , particles contributing to the force network as a function of the packing fraction,  $\phi$ , for two sets of  $(\delta, X_S)$ .

parent jump in  $Z_{SS}$  and  $Z_{mix}$ , see Fig. 2 (a), indicating that a fraction of them start contributing in a discontinuous fashion to the already jammed structure of large ones. This clearly suggests that the line of jammed states encountered at high  $X_S$  need to be extended at lower  $X_S$  values as well in this case.

Since it is difficult to identify where  $Z_{SS}$  jumps for smaller  $X_S$ , we have quantified the fraction of large,  $n_L$ , and small particles,  $n_S$ , contributing to the force network as a function of  $\phi$  giving a clearer jump compared to  $Z$ . A clear decoupling between  $n_L$  and  $n_S$  at lower  $\delta$  and  $X_S$  can be seen in Fig. 2 (e), while for higher values of

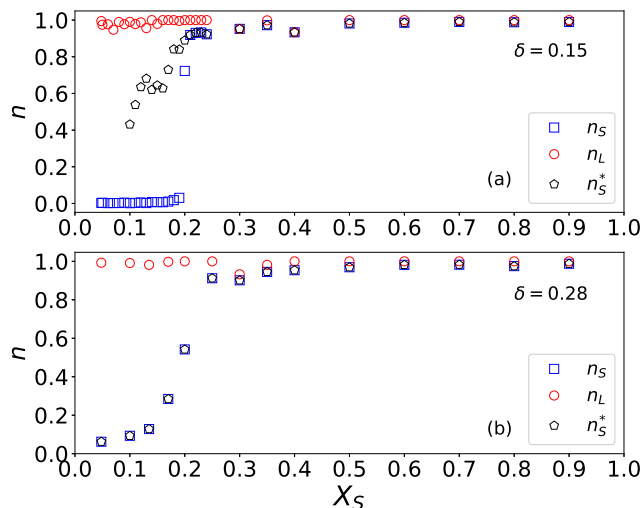


FIG. 3. Fraction of small,  $n_S$ , and large particles,  $n_L$  contributing to the jammed structure as a function of the concentration  $X_S$  of small particles for (a)  $\delta = 0.15$  and (b)  $\delta = 0.28$ .  $n_S^*$  represents the fraction of small particles along the additional line.

$\delta$ , both size of particles contribute simultaneously at the jammed structure. Such decoupling indicates that a big amount of small particles are jammed discontinuously at higher densities, which resembles a similar behavior done by large particles at low densities. To extract the precise value of the jamming density where  $n_S$  jumps for low  $X_S$ , we computed the derivative of  $\partial n_S / \partial \phi$  and found a specific density, which corresponds to  $\phi_J$  of the system. Fig. 1 displays such  $\phi_J^c$  values for  $X_S < X_S^* \approx 0.21$  indicated by the increasing line of densities for smaller  $X_S$ . Such a line clearly extends the transition where both size particles are jammed for low range of  $X_S$ , thus introducing a more complete jamming diagram for bidisperse packings.

The result shown in Fig. 1 is quite similar to those previously found in experiments using glass beads [11] and in 3D simulations [9, 10], but they did not investigate the impact of the small particles contribution on the jammed structure for low  $X_S$  values and no additional line was shown. Recent work [8] which has studied the statistics of the small particles in the jammed structure of bidisperse system in more detail, showed that indeed the fraction of small particles contributing to the jammed structure decays to zero for  $X_S < X_S^*$ , which becomes discontinuous as  $\delta$  decreases. This allows to make a distinction between two states, one where small particles contribute to the jammed network jointly with large ones ( $X_S \geq X_S^*$ ) and the second one where only large particles contribute ( $X_S < X_S^*$ ). We have found that besides these two results, there is an additional line emerging at  $X_S \approx X_S^*$ . Such line represents a jammed state,  $\phi_J$ , extending at higher densities. In addition, we found that

such line starts emerging for  $\delta < 0.22$  where its end-point terminates at lower  $X_S$  as  $\delta$  decreases.

The additional transition line obtained is a result of the decoupling of the jamming transition between large and small particles for low  $X_S$  and low  $\delta$ . Such a scenario can be understood by a model introduced by Furnas almost a century ago [21] to predict the highest density of aggregates entering in the manufacture of mortar and concrete. This model suggests that if the size ratio of the particles are extreme ( $\delta \rightarrow 0$ ),  $\phi_J$  can decouple in two limits sharing a common point at  $\hat{X}_S^*$ . One limit considers an approximation where large particles dominate the jammed structure while small particles are not taken into account since the number of them are not enough to play a role ( $0 \leq X_S < \hat{X}_S^*$ ). In the second limit, both large and small particles participate in the jammed structure ( $0 \leq X_S \leq 1$ ). In this case, the number of small particles are high enough to drive few large particles to the jammed state. Both limits are written as

$$\lim_{\delta \rightarrow 0} \phi_J(X_S) = \begin{cases} \frac{\phi_{\text{RCP}}}{(1-X_S)} & \text{if } 0 \leq X_S < \hat{X}_S^*, \\ \frac{\phi_{\text{RCP}}}{[\phi_{\text{RCP}} + (1-\phi_{\text{RCP}})X_S]} & \text{if } 0 \leq X_S \leq 1, \end{cases} \quad (1)$$

and are displayed in Fig. 1, which represent the maximum densities that a highly asymmetric binary mixture can achieve while changing the concentration of small particles. Note that this model describes the trend of the data, fitting those values for low  $X_S$  which correspond to the single jammed state. It shows a maximum density of  $\phi_J(\hat{X}_S^*) \approx 0.87$  at  $\hat{X}_S^* = (1 - \phi_{\text{RCP}}) / (2 - \phi_{\text{RCP}}) \approx 0.26$ , which is in reasonable agreement with the value obtained here for  $X_S^c$  at finite  $\delta$ . Interestingly, the model shows an additional transition line right where both limits meet, ending at a density of unity. However, previous works using the Furnas model disregarded the physics behind such additional transition line. In Fig. 1, the additional line given by our simulation data follows qualitatively the theoretical prediction, ending at  $X_S^0 = 0.1$  for the lowest  $\delta$ . The transition line obtained from simulation stops at this value since for  $X_S < X_S^0$  no jump in  $n_S$  and  $Z_{SS}$  was found, instead these quantities increase continuously in this region, not showing features of a jump transition. This allows us to argue that the additional transition line terminates in an end-point at some finite  $X_S^0$ , which depends on  $\delta$ .

The evolution of the fractions of small and large particles that contribute to the jammed structure,  $n_S$  and  $n_L$ , along the jamming lines elucidates the different nature of the transitions, i.e., by discussing the jump heights in these quantities as the jamming transition is crossed. These ratios are shown in Fig. 3 for two representative values of  $\delta$ . Here, we extracted  $n_S$  and  $n_L$  from the points where the large-particle contribution jumps, and  $n_S^*$  from those where the small-particle contribution jumps. The existence of the additional transition line is now mani-

fested in the cases where  $n_S^*$  splits from  $n_S$ , see Fig. 3 (a) at low  $X_S$ . Close to the crossing point where the additional transition line emerges, the difference between  $n_S$  and  $n_S^*$  is largest. For lower  $X_S$ , the second jump  $n_S^*$  has to be compared with the value  $n_S$  that is increasing regularly with packing fraction after the first transition: Once  $n_S$  and  $n_S^*$  become of equal value, no more second jump can be identified the endpoint of the additional transition line reached. Technically, such a cessation of a second jump is more difficult to identify precisely than a clearly developed second jump close to the crossing point which explains the fluctuations in Fig. 3. The sharp rise in  $n_S$  around  $X_S^* \approx 0.21$  has been noted before [8] and connected with a “sub-jamming” transition. It can be seen as a natural consequence from the crossing of a line with a finite jump in  $n_L$  and a line with a finite jump in  $n_S^*$ . For  $\delta = 0.28$ , Fig. 3 (b),  $n_S^*$  and  $n_S$  merged into one line at lower  $X_S$  suggesting that no additional transition line is found, see Fig. 1.

To summarize, we have shown that the jamming diagram in bidisperse packings is enriched by an additional transition. This transition appears for  $X_S < X_S^*$  when small particles get in contact with the jammed structure already formed by large particles. The data for the lowest size asymmetry,  $\delta = 0.15$ , is well described analytically by the Furnas model which predicts a similar additional line.

The results presented in Fig. 1 demonstrate an interesting connection to the glass-glass transition phenomenology experienced by a binary colloidal suspensions previously found in [22]. The emergence of such a transition was found through a bifurcation line when the whole range of  $\delta$  and  $X_S$  was explored. Similarly, small species become arrested when the system is becoming denser, thus separating two glassy states in the system. This clearly shows a surprising relation between a bidisperse granular system and a bidisperse colloidal system approaching the jamming density and the glass transition, respectively.

The extension of the jamming line that we found here gives a mathematically rigorous definition of the “sub-jamming” transition, a term introduced in Ref. [8]. There, the crossing point  $(\delta_c, X_S^*)$  has been interpreted as showing the hallmarks of a critical end-point akin to those of phase transitions. However, as it is evident here, this point is rather a *crossing* point of two bifurcation lines, forming part of a more general bifurcation diagram. Mathematically speaking, both jamming lines that cross here can continue until their respective end-points, which need not coincide with  $(\delta_c, X_S^*)$ . This additional transition line signals sub-jamming, i.e., small particles are

inside the interstices of an already jammed structure of large particles. Increasing  $\delta$ , the additional transition line shrinks, so that at some critical  $\delta_c$ , the end-point and crossing-points coincide,  $X_S^o(\delta_c) = X_S^*$ . This (a point of “higher order bifurcation” [23]) will mark the critical point whose signature was discussed in Ref. [8].

We thank T. Kranz, P. Born, L. Elizondo-Aguilera and Th. Voigtmann for helpful discussions about the results. This work was supported by the German Academic Exchange Service (DAAD).

- 
- [1] H. Zhang and H. Makse, Phys. Rev. E **72**, 011301 (2005).
  - [2] E. Aharonov and D. Sparks, Phys. Rev. E **60**, 6890 (1999).
  - [3] M. van Hecke, J. Phys. Condens. Matter **22**, 033101 (2009).
  - [4] R. P. Behringer and B. Chakraborty, Rep. Prog. Phys. **82**, 012601 (2018).
  - [5] C. S. O’Hern, L. E. Silbert, A. J. Liu, and S. R. Nagel, Phys. Rev. E **68**, 011306 (2003).
  - [6] T. S. Majmudar, M. Sperl, S. Luding, and R. P. Behringer, Phys. Rev. Lett. **98**, 058001 (2007).
  - [7] A. Donev, S. Torquato, F. H. Stillinger, and R. Connelly, J. Appl. Phys. **95**, 989 (2004).
  - [8] I. Prasad, C. Santangelo, and G. Grason, Phys. Rev. E **96**, 052905 (2017).
  - [9] A. B. Hopkins, Y. Jiao, F. H. Stillinger, and S. Torquato, Phys. Rev. Lett. **107**, 125501 (2011).
  - [10] I. Biazzo, F. Caltagirone, G. Parisi, and F. Zamponi, Phys. Rev. Lett. **102**, 195701 (2009).
  - [11] S. Pillitteri, G. Lumay, E. Opsomer, and N. Vandewalle, Sci. Rep. **9**, 7281 (2019).
  - [12] N. Kumar and S. Luding, Granul. Matter **18**, 58 (2016).
  - [13] N. Kumar, V. Magnanimo, M. Ramaoli, and S. Luding, Powder Technol. **293**, 94 (2016).
  - [14] P. A. Cundall and O. D. Strack, Géotechnique **29**, 47 (1979).
  - [15] C. Thornton, Particuology **8**, 119 (2010).
  - [16] C. Thornton and L. Zhang, Géotechnique **60**, 333 (2010).
  - [17] S. Luding, Granul. Matter **10**, 235 (2008).
  - [18] N. Kumar, S. Luding, and V. Magnanimo, Acta Mech. **225**, 2319 (2014).
  - [19] F. Göncü, O. Durán, and S. Luding, C. R. Mécanique **338**, 570 (2010).
  - [20] Configurations from the decompression branch are more reliable since they are much less sensitive to the protocol and rate of deformation during preparation, see [19], but the  $\phi_J$  does then depend on the maximum  $\phi_{\max}$  [12].
  - [21] C. Furnas, Ind. Eng. Chem. Res. **23**, 1052 (1931).
  - [22] T. Voigtmann, EPL **96**, 36006 (2011).
  - [23] V. I. Arnol’d, *Catastrophe Theory*, 3rd ed. (Springer, Berlin, 1992).